

Structural Evaluation of Ribbed Barrel Vaults in Bahri Mamluk Religious Buildings: A case Study on the Main Iwan of Sultan Hassan Madrasa, Cairo, Egypt

Doaa E. HUSSEIN¹
Yaser Y. ABDEL-ATY²

Faculty of Archaeology, Cairo University,
Egypt

[1 doaae997@cu.edu.eg](mailto:doaae997@cu.edu.eg)
[2 yaser_yehya@cu.edu.eg](mailto:yaser_yehya@cu.edu.eg)

ARTICLE INFO

Article history

Received 19 September 2023

Received in revised form 15 April 2024

Accepted 30 June 2024

Available Online 8 February 2025

KEYWORDS

Barrel Vault, Ribs, Masonry, Iwan,
Evaluation, Strengthening

ABSTRACT

This paper presents a structural evaluation of the unreinforced masonry ribbed barrel vaults (UMRBV) in Bahri Mamluk religious buildings in Historic Cairo. The research evaluates the structural functions of ribs in UMRBV by comparing its structural stability under various expected loading conditions with non-ribbed vaults. The aforementioned structural analysis is applied to the vault of the main iwan of Sultan Hassan Madrasa, the largest iwan in Historic Cairo. This research starts with a brief historical and architectural study. I conducted a building material investigation of the iwan using XRD, PLM and SEM-EDX. A comprehensive structural analysis employing a finite element method is conducted on the iwan using well-established software (SAP2000, Release 20). The study also incorporated a comparative analysis of iwan models with and without ribs, employing both 3D-shell and solid elements within the chosen software. The results demonstrate a substantial improvement in the structural performance of ribbed models compared to their non-ribbed counterparts. This enhancement is evident in a reduction of up to 46.5% in deflections and up to 44.2% in stresses, observed under static and dynamic loading conditions. Based on the results obtained, a concise recommendation for strengthening methods is proposed.

INTRODUCTION

This study investigates iwans, a common architectural feature in Bahri Mamluk religious buildings in Historic Cairo (H.C.), which were typically covered by Unreinforced masonry barrel vaults (UMBV) (Rahman 2015). A survey conducted as part of this research revealed a considerable variation in the size of the vaults of these iwans. As illustrated in Fig. 1, these vaults exhibited a range of sizes, ranging from small iwan (2-3 meters) (Fig. 1-a, b) to medium iwan (5-8 meters) (Fig. 1-c, d, e) and large iwan (10-23 meters) (Fig. 1-f, g). Notably, shallow vaults, characterised by a width greater than their length, were preferred for smaller areas due to their structural stability. On the other hand, unreinforced masonry ribbed barrel vaults (UMRBV) were used for deeper spans, where additional ribs were required to support the structure and ensure its integrity (Abouseif 1992).

UMRBVs were constructed using materials such as ashlar and rubble stone; the rubble vaults were often finished with a lime plaster coating (Abdelkader 2022). Furthermore, these ribbed vaults depended on main arches to support the vault itself, usually located at the

entrances and ends (Abouseif 1992; Elyamani 2016) (Fig. 2-a). To improve the aesthetic appeal of the arches, the stones are often left exposed, showcasing their natural colours through a decorative technique known as the “*Mush-her*” system, which features alternating courses of yellow and red stones, a method common during the Mamluk period (Abdelkader 2022). The vaults are composed of several ribs (Abdel-Aty 2004).

The ribs function as essential components in the design of vaults, playing a critical role in enhancing structural stability (Acland 1972). These ribs may either extend above the vault's surface, as illustrated in Fig. 1-g, Fig. 2-b, or be integrated within the vault's thickness, thereby contributing to the overall aesthetic of the structure (Fitchen 1981). They were constructed from robust stone blocks to increase the vault's stiffness compared to URM slabs (Abdel-Aty 2004). and were positioned perpendicular to the vault's axis, thus improving their load-bearing capacity. They connect to the vault through specialised keystone blocks, which integrate both the slabs and the ribs. These keystone blocks are uniformly distributed around the periphery of the ribs, ensuring an even load distribution across the structure (Fig. 2-c) (Rahman 2015).

Moreover, the ribs have a significant impact on improving load distribution across URM slabs by directing loads towards them and concentrating the stresses in the ribs' direction. This system is known as "one-way slabs" (Fig. 2-d), where the ribs facilitate the transfer of loads to the load-bearing walls and subsequently to the foundations, thus reducing stresses to the slab between the ribs (Abdel-Aty 2004). In contrast, vaults without ribs distribute loads across their sides, resulting in a transfer of stresses to the load-bearing walls and foundations. This process increases the stresses within the vault's structure (Fig. 2-e), potentially leading to cracking and necessitating thicker construction. This highlights the importance of ribs in the structural design of vaults (Hejazi et al. 2023).

Side lintels hold a key position in supporting walls and transferring loads to the foundations. These stone lintels, positioned parallel to the walls, help distribute loads and enhance the structural stability of the vault (Abdel-Aty 2004) (Fig. 1-c, e). The angles of the vaults, roughly ranging 15 degrees, are vital for maintaining structural integrity and are dependent on the vault's size (Fraddosio et al. 2020).

Numerous researchers have explored different aspects of masonry vaults, including architectural design, construction techniques, and structural analysis. For instance, Cardinali et al. (2023) and Hejazi et al. (2023) studied the behaviour of masonry barrel vaults through experimental and analytical approaches, while Bianchini et al. (2023) analysed the effects of earthquakes on vaults and proposed strengthening methods. Günday (2023) examined seismic reinforcement techniques, and Chen et al. (2023) investigated the vulnerability of pointed masonry vaults under differential settlement. Moreover, studies like those conducted by Galera and Baño (2022) and Nela et al. (2022) used photogrammetric surveys to explore vault geometry and design. Boem and Gattesco (2021) contributed to experimental and analytical insights into masonry vault behaviour, while Angjeliu et al. (2021) and Xiang et al. (2021) provided numerical verifications of mechanical damage in ribbed masonry vaults. Fraddosio et al. (2020) introduced innovative analytical techniques for assessing masonry vaults.

Despite this extensive research, studies focusing on large UMRBVs in Bahri Mamluk buildings remain limited (Abdel-Aty 2004; Abdelkader 2022). The structural behaviour of these large vaults is expected to deviate significantly from conventional smaller vaults due to their size and complexity. Therefore, this research concentrates on one of Egypt's largest and most significant UMRBVs: the main iwan of Sultan Hassan Madrasa.

This paper aims to cover the following objectives:

- Study and evaluate UMRBV in Bahri Mamluk religious buildings in H.C. from an architectural, construction, and structural point of view.
- Highlight and assess the structural role of ribs in UMRBV by comparing their stability under various loading conditions to non-ribbed vaults.
- Investigate one of the largest and most prestigious UMRBVs in Egypt, e.g., the main iwan of Sultan Hassan Madrasa.
- Conduct building material analysis of the iwan using advanced techniques, including X-ray diffraction (XRD), polarised light microscopy (PLM), and scanning electron microscopy (SEM) with energy-dispersive X-ray spectroscopy (EDX), to accurately identify materials and adapt mechanical properties from previous research while adhering to local regulations.
- Utilise finite element analysis (F.E.M.) to model the main iwan and compare its structural performance with a proposed non-ribbed vault under linear static conditions (self-weight) and preliminary dynamic analysis (eigenvalue analysis and linear response spectrum).
- Compare numerical modelling approaches (shell and solid) to evaluate accuracy and performance differences.
- Propose strengthening methods for zones showing cracks or unsafe stresses to improve the structural performance of the vault.

1. THE CASE STUDY

The present research conducts the structural study of the main iwan of Sultan Hassan madrasa. The madrasa was built in 757- 764 AH (1356-1363 AD) (Fig. 1-h) by Sultan al-Nasir Hassan, a governor in the Bahri Mamluk period. The madrasa is located on Salah al-Din Square (Gaber 2021). It is numbered 133 on the list of archaeological buildings in Cairo (Howard 2014). Its main iwan is one of the hugest barrel vaults in Egypt and an awe-inspiring achievement due to its size, which resembles the famous vault of the Sassanid Persian palace of Ctesiphon (still the largest URMV worldwide) (Abouseif 1992) (Woo 2020). Its architecture follows the style of the Gothic era (Anderson 1991) (Abdelkader 2022) (Dutton 2019).

1.1 ARCHITECTURAL OVERVIEW OF THE MAIN IWAN

The main iwan has a simple rectangular plan measuring 21m (width) x 26m (length) x 24m (height), as shown in Fig.3-a & 3-b (Archnet 2024). The thickness of the main arch located at the entrance is 2.20 m and rises to 12.5 m. It is built of coloured ashlar units in red/yellow mutual courses. Moreover, the original shape of the main iwan from the book *Egypt* by Coste is shown in Fig. 3-c (Dutton 2019), which illustrates the construction technique by buried ribs distributed along its length. The buried ribs are built of robust ashlar limestone blocks embedded within their thickness, which thus possess higher stiffness than slabs in between (Fig. 3-d) (Anderson 1991) (Abdelkader 2022). The building follows the structural system of load-bearing masonry walls (Amer 2017). Its walls are constructed of limestone multiple-leaf work, with thickness ranging from 2.76 m to 3.75 m.

1.2 STRUCTURAL FAILURES OF THE MAIN IWAN

A detailed visual observation of the main iwan confirms that it is currently stable and in structurally sound condition under permanent static loads. However, several structural failures

have been identified, as shown in Fig. 4:

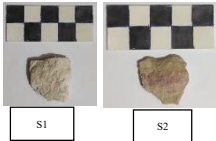

- Cracks in the main arch (Fig. 4-a), at the corners of the vault, and along the mid-span (Fig. 4-b, c, d, e): These cracks are possibly the result of past seismic activity, most notably the 1992 earthquake (Elyamani et al., 2023). Similar damage patterns have been reported in other historical structures exposed to seismic forces, as outlined in Fraddosio et al. (2020). These authors present studies on the impact of earthquakes on unreinforced masonry (URM) vaults and explain how cracks typically appear in the arches and at mid-span while Puncello et al. (2023) and Bianchini et al. (2023) discuss seismic damages to vaults and explain that earthquakes can cause cracks in these sensitive zones.
- Restoration work on the vault (Fig. 4-f & 4-g): it was carried out to address the identified cracks. Although these structural repair aimed to avoid further degradation, they may not have fully resolved the underlying structural weaknesses (Abdel-Aty, 2004; Genç et al., 2020).
- Deterioration in load-bearing walls: Significant degradation is observed in most of the load-bearing walls, primarily due to groundwater. Previous studies indicate that H.C. experienced increases in groundwater levels, causing the deterioration of masonry structures and possibly weakening the iwan's structural integrity. This is confirmed by research on the effects of groundwater on masonry buildings (Ismail, 2010; Elyamani et al., 2023; Coisson et al., 2019).

2. MATERIALS AND METHODS:

2.1. MATERIALS ANALYSIS

2.1.1. SAMPLING:

To gain insights into the material composition of the main iwan, petrographic analysis was performed on four samples—two limestone and two mortar—extracted from Sultan Hassan Madrasa in Cairo. This analysis enabled the adoption of mechanical properties from prior research, which were essential for the subsequent structural analysis and evaluation. The samples listed in Table 1 were collected with the following identifying factors: their source, current state, and dimensions.

Table 1. Samples description (Codes, sample number and source, current state and dimensions)					
Type	Code	Number	Location	State and Dimensions	Picture
Stone	S	2	Falling parts of the iwan	Irregularly shaped	
Mortar	M	2	Mortar between stone blocks (Hidden parts)	Small fragments	

2.1.2. ANALYTICAL TECHNIQUES

2.1.2.1. X-RAY DIFFRACTION (XRD)

X-ray Diffraction (XRD) was made using the Bruker D8 Discover XRD model to identify the primary minerals and materials in the stone and mortar samples.

As shown in Fig. 5, the two stone samples were composed of calcite (CaCO_3) and dolomite [$\text{CaMg}(\text{CO}_3)_2$]. Hematite (Fe_2O_3) and quartz (SiO_2) were found on the crusts of the samples. Halite (NaCl) was found in decay or impurities (less than 15%) (Fig. 5-a, 5-b).

As for the mortar samples, the mortar used in the stone-masonry vaults was lime-based, with its major components being calcite (CaCO_3) and dolomite [$\text{CaMg}(\text{CO}_3)_2$]. Quartz (SiO_2) was identified as the aggregate in the form of sand. Gypsum ($\text{CaSO}_4 \cdot 2\text{H}_2\text{O}$) and hematite (Fe_2O_3) were likely added to improve strength. Halite (NaCl) was observed as salt (Fig. 5-c, 5-d).

2.1.2.2. POLARISING PETROGRAPHIC MICROSCOPE

An analysis using the NIKON ECLIPSE LV 100 POL x100 model with a photo camera DS-Fil was conducted under cross-polarised light (Fig. 6) and showed the following results:

- Sample S1 was identified as fine-grained limestone mainly composed of carbonate minerals. Calcite was the most common, followed by dolomite. S1 also contained minor amounts of quartz and iron oxides. The matrix included microfossils, such as nummulites and shells, which were filled with recrystallised carbonate minerals. Visible pore spaces were present (Fig. 6-a).
- Sample S2 was primarily composed of fine-grained calcite and carbonate, with small amounts of dolomite, quartz, and iron oxides. Some microfossils were filled with micritic calcite (Fig. 6-b).

These observations aligned with the mineral characteristics of Mount Mokattam (Coppola et al. 2020; Egerton 1854) and were consistent with previous studies (Kendall and Flood 2011; Elkarim 2017; Hemeda et al. 2019), suggesting a proximity quarry.

2.1.2.3. SEM-EDX ANALYSIS

The SEM-EDX analysis aimed to examine the morphology and microstructure of minerals in the stone and mortar samples. The EDX analysis identified the minerals elements, which support the above results. The samples were analysed using a Quanta 250 FEG microscope with an EDX unit. The results are shown in Fig. 7.

- Stone samples contained calcite, dolomite, quartz, and halite crystals (sodium chloride) with traces of gypsum. The carbonate minerals (calcite and dolomite) were found to have calcium (Ca), magnesium (Mg), carbon (C), and oxygen (O). Quartz was composed of silicon (Si) and oxygen (O), while halite was made of chlorine (Cl) and sodium (Na) (Fig. 7-a).
- Mortar Samples: The mortar contained gypsum and anhydrite ($\text{CaSO}_4 \cdot 2\text{H}_2\text{O}$ and $\text{CaSO}_4 \cdot 0.5\text{H}_2\text{O}$), with elements like carbon (C), sulfur (S), and oxygen (O). It also included kaolinite ($\text{Al}_2\text{Si}_2\text{O}_5(\text{OH})_4$), which had aluminum (Al), and silicon (Si). The mortar was lime-based, with calcite as the main component, and quartz crystals

dispersed throughout. Sodium chloride was found in the pores in a dissolved state. The presence of carbonate ($\text{CaMg}(\text{CO}_3)_2$ and CaCO_3) was due to calcium (Ca), oxygen (O), magnesium (Mg), and carbon (C). Chloride and sulfate salts (NaCl and CaSO_4) were also present due to sodium (Na), sulfur (S), and chlorine (Cl). Impurities were influenced by silicon (Si) and oxygen (O) from quartz (Fig. 7-b).

Elemental Composition (Fig. 8):

- Stone Samples (S): The EDX analysis showed calcium (Ca) (43.5%), carbon (C) (8.6%), oxygen (O) (37.5%), silicon (Si) (1%), and magnesium (Mg) (0.5%). Salt and clay contained sodium (Na) (25.1%), chlorine (Cl) (50.9%), sulfur (S) (5.9%), and aluminum (Al) (0.6%).
- Mortar (M): The mortar had sodium (Na) (8.3%), chlorine (Cl) (13%), sulfur (S) (15.7%), calcium (Ca) (23.9%), silicon (Si) (25.7%), oxygen (O) (48.5%), and carbon (C) (3.7%). This result indicated that the mortar was likely lime-based.

The petrographic analysis results matched previous studies, which identified the limestone and mortar properties (Amer 2017; Amer et al. 2020; Abdel-Aty 2019). Table 2 provides the main properties and allowable stresses for building materials used in the structural analysis of the case study building (Abdelmegeed et al. 2019; Abdel-Aty 2004; Abdel-Aty 2019). These values were based on earlier research (Amer et al. 2020; Amer et al. 2021; Abdel-Aty 2021; Elyamani et al. 2023; ECP 204-2005; Elyamani et al. 2021).

Table 2. Properties of materials (strength and allowable 'working' stresses).

Material	Bulk density (ρ) (KN/m ³)	Elasticity modulus (E) (N/mm ²)	Comp. Strength (N/mm ²)	Comp. all. Stress (N/mm ²)	Tensile strength (N/mm ²)	Shear all. stress (N/mm ²)	Poisson's ratio ν
Limestone	21	7000	22	5.5	2	NA	0.25
StoneMasonry	20	3000	5.0	1.2	NA	0.5	0.27
Lime mortar	17	10	2.0	0.4	0.15	NA	0.30

2.2. STRUCTURAL MODELLING AND ANALYSIS

A structural analysis of the main iwan was conducted, utilising 3D numerical models, to serve as a representative case study for UMRBVs in Cairo. The analysis relied on SAP2000 (Release 20), which uses the codes of the finite element method (F.E.M.).

The objective of the analysis was to assess the stability of these structures and to determine and evaluate the role of the ribs in enhancing their stability. Therefore, the stresses and deformations between the current iwan model and a proposed non-ribbed model (i.e., following the full dimensions and design) were compared under static, i.e., the dead load of self-weight (D.L.) only, and dynamic (i.e., eigenvalue and linear response-spectrum) loads cases. They were modelled using two types of shell and solid elements in the analysis software (SAP2000(Release 20)):

- **MODELLING SHELL AND FRAME ELEMENTS:**

Shells were utilised to represent the walls and vault, while frame elements were employed to model the arches. The shell model comprised 5,554 shell elements, each with

a maximum size of 0.5 m × 0.5 m and a total of 5,670 nodes. This model is shown in Fig. 9-a. It focuses on evaluating performance under static and dynamic loads.

- **MODELLING SOLID ELEMENTS:**

Another model was created using the software's solid elements to represent the same architectural components (walls, arches, and vault). After meshing, the solid model included 58,834 solid elements and 67,599 joints. This model is depicted in Figure. 9-b. It provides a more detailed assessment of performance.

A comparative analysis was performed between models using two distinct modelling approaches (shell and solid), with material properties, as outlined in Table 3, applied consistently across all models. Finally, a strengthening method was proposed according to the results of the analysis.

3. STRUCTURAL ANALYSIS AND EVALUATION

The structural analysis of the models under a static load, which includes only the self-weight and dynamic load (i.e., eigenvalue and linear response spectrum), confirmed that all models adhered to the allowable stresses and deformations limits listed in Table 3. These results are illustrated in Fig. 10 and 12.

3.1. STATIC LINEAR ANALYSIS

3.1.1. SHELL MODELS ANALYSIS

In the analysis of shell models, the addition of ribs (Model 1) resulted in significant improvements compared to the non-ribbed models (Model 2). Specifically, ribbed shell models showed a 15.6% reduction in deformations, indicating better structural stability. Also, the static linear analysis exhibited major reductions in various types of stresses with the introduction of ribs: compressive stresses decreased by 38.3% (S11) and 16.5% (S22), tensile stresses decreased by 15% (S11) and (S22), and maximum stresses decreased by 39.6% (Smax). The inclusion of ribs notably changed the stress distribution, reducing stress concentrations and achieving a more uniform distribution across the shell structure.

3.1.2. SOLID MODELS ANALYSIS

Similarly, the evaluation of solid models showed that adding ribs led to significant improvements compared to non-ribbed models. Ribbed solid models had a 46.5% reduction in deformations, indicating increased structural stiffness. The static linear analysis also showed major reductions in stresses: compressive stresses decreased by 44.2% (S11) and 43.6% (S22), tensile stresses decreased by 49.3% (S11) and 20.9% (S22), and maximum stresses decreased by 44.8% (Smax). The addition of ribs significantly changed how stresses were distributed in the solid structure, reducing stress concentrations and achieving a more balanced load distribution, which improved the overall structural integrity and performance.

Fig. 10 and 11 present these results. Fig. 10 illustrates the distribution of stresses and deformations for both shell and solid models. The blue contours indicate areas of high tensile stresses where cracks are expected, aligning with the cracks, as shown in Fig. 4, thus confirming the accuracy of the models and their simulations. Table 3 highlights the improvements in stress levels and deformations for the ribbed models.

Model Type	Deformations	Compressive Stresses (S11)	Compressive Stresses (S22)	Tensile Stresses (S11)	Tensile Stresses (S22)	Maximum Stresses (Smax)
Shell	-15.6%	-38.3%	-16.5%	-15%	-15%	-39.6%
Solid	-46.5%	-44.2%	-43.6%	-49.3%	-20.9%	-44.8%

3.2. DYNAMIC LINEAR ANALYSIS USING EIGENVALUE AND RESPONSE SPECTRUM METHODS

3.2.1. MODE SHAPES ANALYSIS

The results of the dynamic linear analysis, depicted in Fig. 12, illustrated the first three primary modes identified through eigenvalue analysis for all models. These modes included bending in the x and y directions, as well as torsion modes.

3.2.1.1. SHELL MODELS ANALYSIS

In Mode 1, the ribbed shell model had a mode shape value of 0.746206, while the non-ribbed shell model had a higher value of 0.796495. This direction was consistent across several modes, demonstrating that ribbed models consistently outperformed non-ribbed ones in dynamic behaviour, as shown in Fig. 13-a.

3.2.1.2. SOLID MODELS ANALYSIS

Similarly, in Mode 1, the ribbed solid model showed a mode shape value of 0.441534, while the non-ribbed solid model had a higher value of 0.552906. This improvement in mode shape values continued throughout the analysis, confirming the enhanced performance of ribbed solid models, as shown in Fig. 13-a.

When comparing shell and solid models, the solid models demonstrated better dynamic behaviour. For instance, the ribbed solid model in Mode 1 had a mode shape value of 0.441534, which was lower than the ribbed shell model's value of 0.746206. This difference underscored the superior performance of solid models and the benefits of adding ribs.

3.2.2. RESPONSE SPECTRUM ANALYSIS

The response spectrum analysis further proved the values of using ribbed models in Fig. 12 and 13-b.

3.2.2.1. X-DIRECTION RESPONSE SPECTRUM

In the S11 response spectrum, the ribbed shell model showed a reduction from 0.79 to 0.557, about 30%. However, the ribbed solid model exhibited a decrease from 10.8 to 8.8, about 18%. Furthermore, the S22 response spectrum revealed that the ribbed shell model decreased from 0.6 to 0.45, while the ribbed solid model decreased from 2.94 to 2.4.

3.2.2.2. Y-DIRECTION RESPONSE SPECTRUM

In the S11 response spectrum, the ribbed shell model decreased from 1.99 to 2.37, while the ribbed solid model showed a reduction from 8.53 to 9.95. In addition, the S22 response spectrum demonstrated that the ribbed shell model reduced from 1.69 to 1.52, whereas the ribbed solid model decreased from 2.89 to 2.77.

These reductions in response spectrum values indicated improved structural stability and flexibility to dynamic loads for ribbed structures compared to non-ribbed ones. Moreover, both

ribbed and non-ribbed solid models showed lower response spectrum values compared to shell models, demonstrating better resistance to dynamic loads and enhanced structural integrity.

Overall, the results emphasised the superior performance and resilience of ribbed models, particularly solid models, in dynamic analysis.

3.3. DISCUSSION OF RESULTS

The structural analysis results, both static and dynamic, highlighted major improvements due to ribs, as shown in Fig. 11 and 13.

- **Reduction in Stresses and Deformations:** The addition of ribs resulted in an observed reduction in stresses and deformations compared to non-ribbed models. Specifically, ribbed models showed lower stress levels and deformations (i.e. 44.2% and 46.5% Respectively), which enhanced overall structural stability.
- **Enhanced Structural Stability:** UMRBVs demonstrated improved structural stability. This was evident from the substantial reductions in stress levels and deformations, confirming that ribs played an essential role in stabilising structures.
- **Uniform Stress Distribution:** The incorporation of ribs helped a more balanced distribution of stresses, effectively reducing stress concentrations. Moreover, this even distribution of stress made it possible to use the structures in deep areas, where it is especially important to keep the structure stable.
- **Improvements in Dynamic Behaviour:** Ribbed models exhibited enhanced dynamic behaviour. Lower mode shape values for ribbed structures indicated better performance under dynamic loads. The ribbed models demonstrated enhanced flexibility compared to their non-ribbed equals.
- **Superior Performance of Solid Models:** Solid models outperformed shell models across various parameters. They exhibited lower mode shape values and better resistance to dynamic loads, underscoring their superior structural integrity and capability to capture complex structural behaviour accurately.

4. PROPOSED METHODS FOR STRENGTHENING

A meticulously designed strengthening strategy is essential to enhance the structural integrity and ensure the long-term stability of the main iwan's UMRBV. This approach should prioritise addressing structural vulnerabilities by strategically placing reinforcements in critical areas within the vault.

The use of advanced materials is required, as they offer enhanced strength and durability compared to traditional materials. For instance, incorporating carbon fiber-reinforced cementitious matrix (C-FRCM) (Anania 2013) improves tensile strength and helps distribution loads more effectively. Also, polyparaphenylene-benzobisoxazole fiber-reinforced cementitious matrix (PBO-FRCM) and basalt textile-reinforced mortar (BTRM) (Witzany 2020) provide high flexibility and resistance, making them suitable for the retrofitting of historical UMRBV subjected to dynamic loads and environmental factors.

Besides, to further strengthen the structure, methods of proven techniques can be used. These include fiber-reinforced bonding (FRB) and cinetic hark technology, which enhances the load-bearing capacity of the masonry (Milani 2009). Omega-shaped reinforcement designs can enhance the overall stability by providing distributed loads and minimising stress concentrations in essential areas (Coisson 2019).

Other traditional methods, such as the incorporation of steel sections, stone ribs, crack injection, the rebuilding of compromised sections using high-quality original stone, and diluting the vault's backfill, as proposed by Coïsson (2019), may also help reduce the dead load and stress on the vault's structure.

By integrating these techniques, it is possible to significantly improve the structural integrity of the iwan. These methods not only address immediate structural concerns but also support the preservation of Bahri Mamluk religious buildings in HC for the future.

CONCLUSION

This study of UMRBVs in Bahri Mamluk religious buildings in Cairo has provided crucial insights into their unique structural behaviour. The findings highlight the essential function of ribs in enhancing the stability of these structures by mitigating stress concentrations, which is crucial for their preservation.

The petrographic analysis confirmed that construction materials, sourced primarily from Mokattam quarries, along with lime-based mortar, contributed significantly to the vaults' mechanical properties and durability. Furthermore, through 3D numerical modelling, it was demonstrated that ribbed vaults exhibit superior performance under both static and dynamic loads. Dynamic analyses particularly revealed that ribbed vaults outperform their non-ribbed counterparts in load distribution and flexibility to seismic activity. The solid modelling approach proved more effective than shell models for accurately capturing the vaults' complex structural responses, making it the recommended method for detailed analysis.

These results highlight the importance of using ribbed vault structures and advanced modelling techniques for a more comprehensive understanding of historical structures. Such insights are invaluable for the preservation and structural assessment of heritage sites. Based on the results of this research, the following recommendations are proposed to ensure the stability and preservation of UMRBVs in historical buildings:

1. It is recommended to implement reinforcement techniques specifically focused on the ribs and major load-bearing areas. These interventions will not only enhance load distribution but also reduce the risk of failure under various loading conditions, including seismic events.
2. Monitoring using advanced investigative tools should be established for signs of deterioration or stress. This will prevent further damage and preserve the structural integrity.
3. Research continues into innovative strengthening techniques, particularly those aimed at improving seismic performance. The study should also focus on long-term performance assessments of these vaults to refine current preservation strategies and develop more effective methods.

BIBLIOGRAPHY:

- Behrens-Abouseif, D. (1992). *Islamic architecture in Cairo: An introduction*. Brill.
- Rahman, M. M. (2015). Islamic architecture and arch. *International Journal of Built Environment and Sustainability*, 2(1), 8–16. <https://doi.org/10.11113/Ijbes.V2.N1.52>
- Elyamani, A. (2016). The adobe barrel vaulted structures in ancient Egypt: A study of two case studies for conservation purposes. *Mediterranean Archaeology and Archaeometry*, 16, 295–315.
- Acland, J. H. (1972). *Medieval structure: The Gothic vault*. University of Toronto Press.
- Fitchen, J. (1981). *The construction of Gothic cathedrals: A study of medieval vault erection*. University of Chicago Press.
- Alexakis, H., & Makris, N. (2014). Limit equilibrium analysis of masonry arches. *Archive of Applied Mechanics*, 85(9–10), 1363–1381. <https://doi.org/10.1007/S00419-014-0963-6>
- Abdel-Aty, Y. (2004). *Analysis and assessment of structural deficiencies in historical Islamic religious buildings from Bahri Mamluk period and the possible scientific methods for conservation and restoration with application on the "Madrasa of Umm Al-Sultan Sha'ban" in Cairo* (Ph.D. thesis, Cairo University, Faculty of Archaeology, Conservation Dept.).
- Archnet > Site > Baybars Al-Jashankir. (n.d.). Retrieved from https://archnet.org/sites/1549/media_contents/6395
- Abdelkader, N. M. (2022). The psychology of architectural design of Mamluk religious buildings in Cairo (648-923 A.H./1250). 425-466.
- Cardinali, V., Pintucchi, B., Tanganelli, M., & Trovatelli, F. (2023). Settlement of masonry barrel vaults: An experimental and numerical study. *Procedia Structural Integrity*, 44, 1252–1259. <https://doi.org/10.1016/j.prostr.2023.01.161>
- Hejazi, M., & Rajaei, A. (2023). Preliminary results of parametric study of structural behaviour of Persian brick masonry groined multipartite (Tarkin) vaults. *Construction and Building Materials*, 372, 130826. <https://doi.org/10.1016/j.conbuildmat.2023.130826>
- Bianchini, N., Mendes, N., Calderini, C., & Lourenço, P. (2023). Effects of earthquakes with different nature on the seismic performance of masonry vaults. *Procedia Structural Integrity*, 44, 1244–1251. <https://doi.org/10.1016/j.prostr.2023.01.160>
- Tarhan, İ. H., & Uysal, H. (2023). Topology optimization of the FRP for strengthening of masonry barrel vaults. *Engineering Failure Analysis*, 151, 107390. <https://doi.org/10.1016/j.engfailanal.2023.107390>
- Günday, F. (2023). Seismic strengthening of stone barrel vault structures by foam concrete. *International Conference on Applied Engineering and Natural Sciences*, 1(1), 920–925. <https://doi.org/10.59287/icaens.1110>
- Chen, X., Ou, W., Chan, A. H. C., Liu, H., & Fukuda, D. (2023). Vulnerability of pointed masonry barrel vaults subjected to differential settlement simulated with a GPGPU-parallelized FDEM. *International Journal of Applied Mechanics*, 15(07). <https://doi.org/10.1142/S175882512350059X>
- Salcedo-Galera, M., & García-Baño, R. (2022). Stonecutting and early stereotomy in the Fatimid walls of Cairo. *Nexus Network Journal*, 24(3), 657–672. <https://doi.org/10.1007/S00004-022-00611-1>

- Nela, B., Jiménez Rios, A., Pingaro, M., Reccia, E., & Trovalusci, P. (2022). Limit analysis of locally reinforced masonry arches. *Engineering Structures*, 271, 114921. <https://doi.org/10.1016/j.engstruct.2022.114921>
- Boem, I., & Gattesco, N. (2021). Cyclic behavior of masonry barrel vaults strengthened through composite reinforced mortar, considering the role of the connection with the abutments. *Engineering Structures*, 228, 111518. <https://doi.org/10.1016/j.engstruct.2020.111518>
- Xiang, S., Cheng, B., Kookalani, S., & Zhao, J. (2021). An analytic approach to predict the shape and internal forces of barrel vault elastic gridshells during lifting construction. *Structures*, 29, 628–637. <https://doi.org/10.1016/j.istruc.2020.11.032>
- Angjeliu, G., Coronelli, D., & Cardani, G. (2021). Numerical analysis of mechanical damage in ribbed masonry vaults under differential settlements. *International Journal of Architectural Heritage*, 16(11), 1742–1759. <https://doi.org/10.1080/15583058.2021.1907482>
- Fraddosio, A., Lepore, N., & Piccioni, M. D. (2020). Thrust surface method: An innovative approach for the three-dimensional lower bound limit analysis of masonry vaults. *Engineering Structures*, 202, 109846. <https://doi.org/10.1016/j.engstruct.2019.109846>
- Ali Ahmed Gaber, A., & Mahmoud Hamada Aly, R. (2021). The architecture of connections in Mamluk architecture: The methodology of design by connection elements in complex buildings in Mamluk eras case-study. *International Design Journal*, 11(6), 93–117. <https://doi.org/10.21608/idj.2021.204927>
- Howard, D. (2014). Mamluk history through architecture: Monuments, culture and politics in medieval Egypt and Syria. *Journal of Architectural Education*, 68(1), 130–131. <https://doi.org/10.1080/10464883.2014.864910>
- Woo, B. (2020). Overview of Islamic art and architecture: The Mamluk period (1250–1517). *International Journal of Humanities and Social Science*, 7(3), 11–15. <https://doi.org/10.14445/23942703/Ijhss-V7i3p104>
- Anderson, S. (1991). Pascal-Xavier Coste (1787–1879): A French architect in Egypt. Retrieved from <http://hdl.handle.net/1721.1/13091>
- Dutton, T. (2019, March 16). Islamic architecture. Retrieved from <https://pin.it/3rs8o5tit>
- Archnet > Site > Masjid Al-Sultan Hasan. (n.d.). Retrieved from https://archnet.org/sites/1549/media_contents/6395
- Amer, O. (2017, August 1). Finite element analyses for seismic performance assessment of historical masonry buildings: The case of Omar-Toson-Palace-Cairo-Egypt. Retrieved from https://www.researchgate.net/publication/317693902_Finite_Element_Analyses_For_Seismic_Performance_Assessment_Of_Historical_Masonry_Buildings_The_Case_Of_Omar_Toson_Palace_Cairo_Egypt
- Elyamani, A., Reda, A., Abdel-Hafez, M., Mourad, S. A., & Hassan, M. M. (2023). Characterization of construction materials of the historic structures in historic Cairo: A case study. *International Journal of Conservation Science*, 14(2), 599–616. <https://doi.org/10.36868/Ijcs.2023.02.15>
- Elyamani, A., Bader, N. A. A. E.-T., Algohary, M., & Hassan, R. A. E. (2021). Explanation of the damage to the royal family’s cemetery in historic Cairo and examination of the building materials. *Open Journal of Civil Engineering*, 11(01), 28–59. <https://doi.org/10.4236/ojce.2021.111003>

FIGURES:

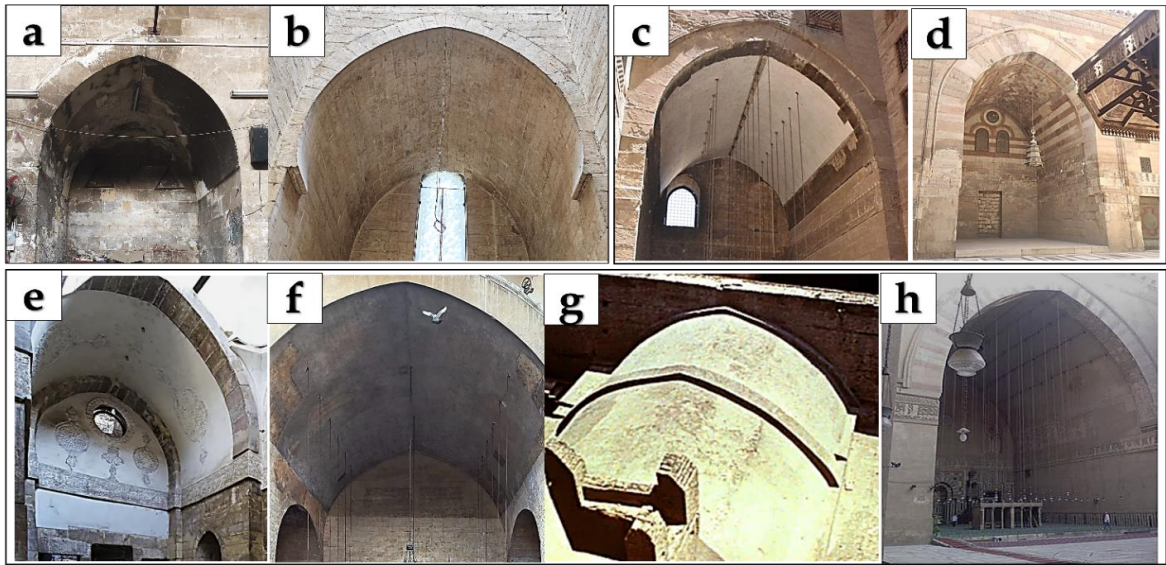


Fig.1 Examples of URM barrel vaults in Bahri Mamluk religious buildings in historic Cairo: a) Salar A.H./1369 A.D.); c)The complex of Sultan Hasan (1363A.D.); d)The Complex of Sultan Barquq (788A.H./1386 A.D.); e) Aqsunqur Mosque (748A.H./1347A.D.); f,g) Baybars Jashankir “*Khanqah*” (709 A.H./ 1310A.D.) inside and outside (Archnet 2024); h)Sultan Hassan Madrasa (788A.H./ 1386 A.D.). (by the authors)

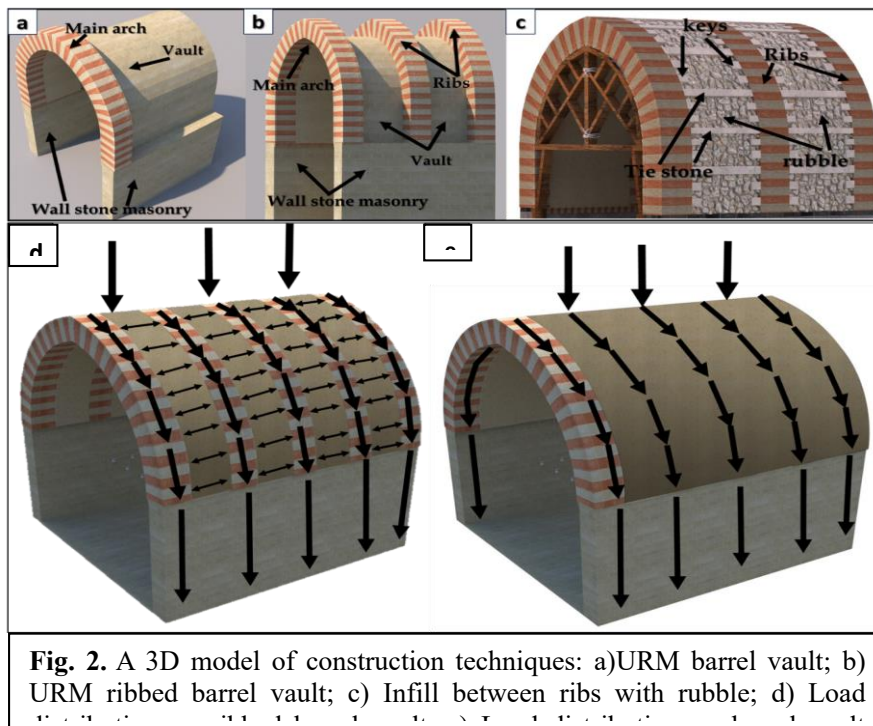


Fig. 2. A 3D model of construction techniques: a)URM barrel vault; b) URM ribbed barrel vault; c) Infill between ribs with rubble; d) Load

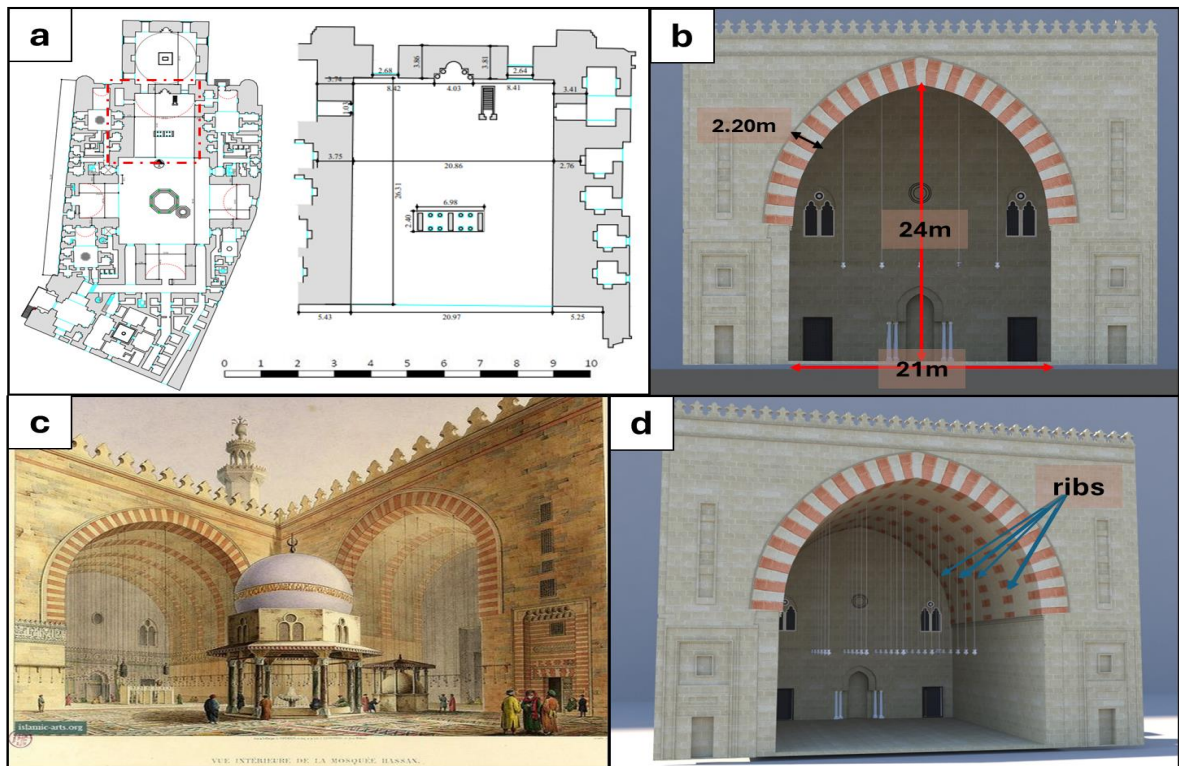


Fig. 3. The main iwan of Sultan Hassan Madrasa: a) Location plan of the iwan (Archnet 2024); b) Dimensions of the iwan; c) Original shape of the main iwan from the book *'Egypt'* by Coste, Cairo 1826 (Anderson 1991); d) Shape of the buried ribs used in the construction of the vault (by the authors).

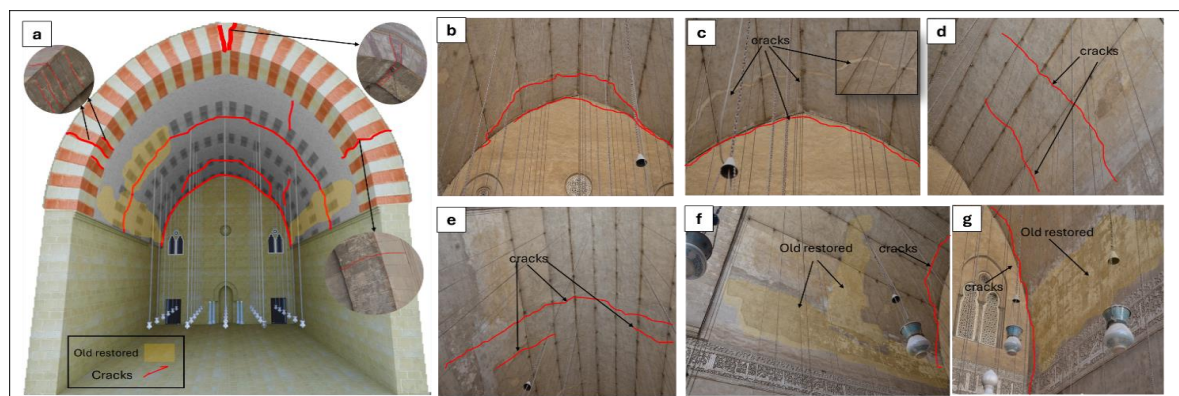


Fig.4. Failures and cracking patterns of the main iwan (by the authors)

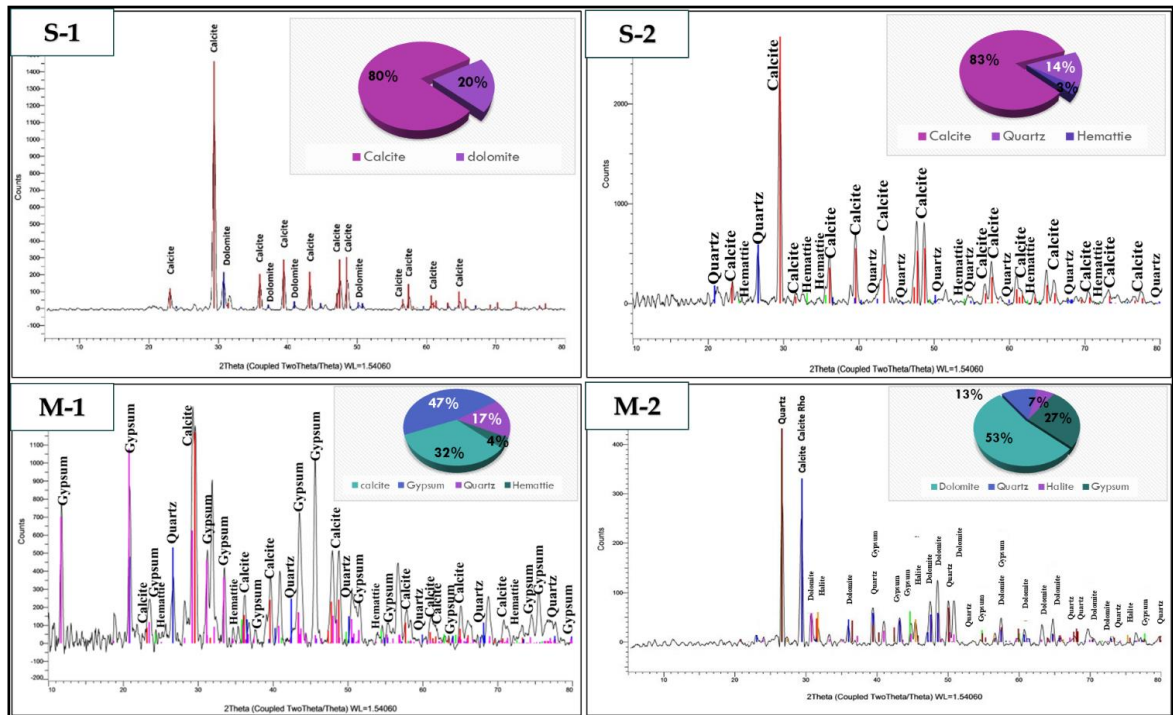


Fig.5. XRD - charts of samples of the case study and ratio mineral components in samples: S-1, S-2) stone samples; M-1,M-2) mortar samples (by the authors).

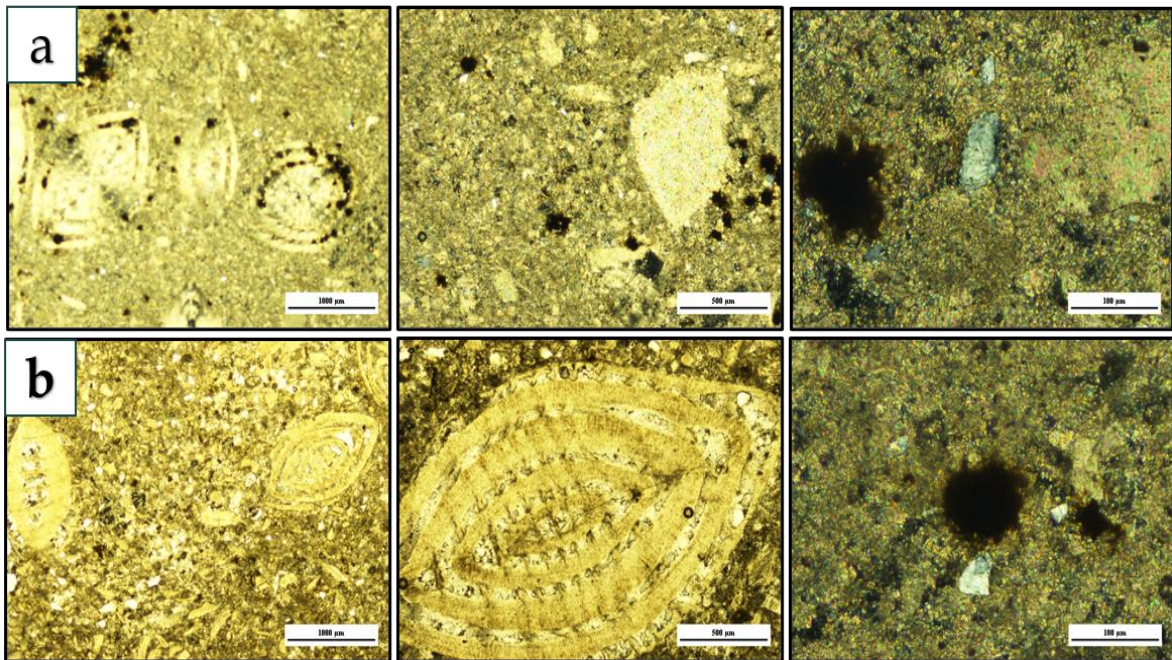


Fig.6. Photomicrograph of thin sections of limestone samples investigated under a polarized microscope (XPL): crystallization carbonate (calcite) and the microfossils and shell fragments a) sample S1; b) sample S2. (by the authors)

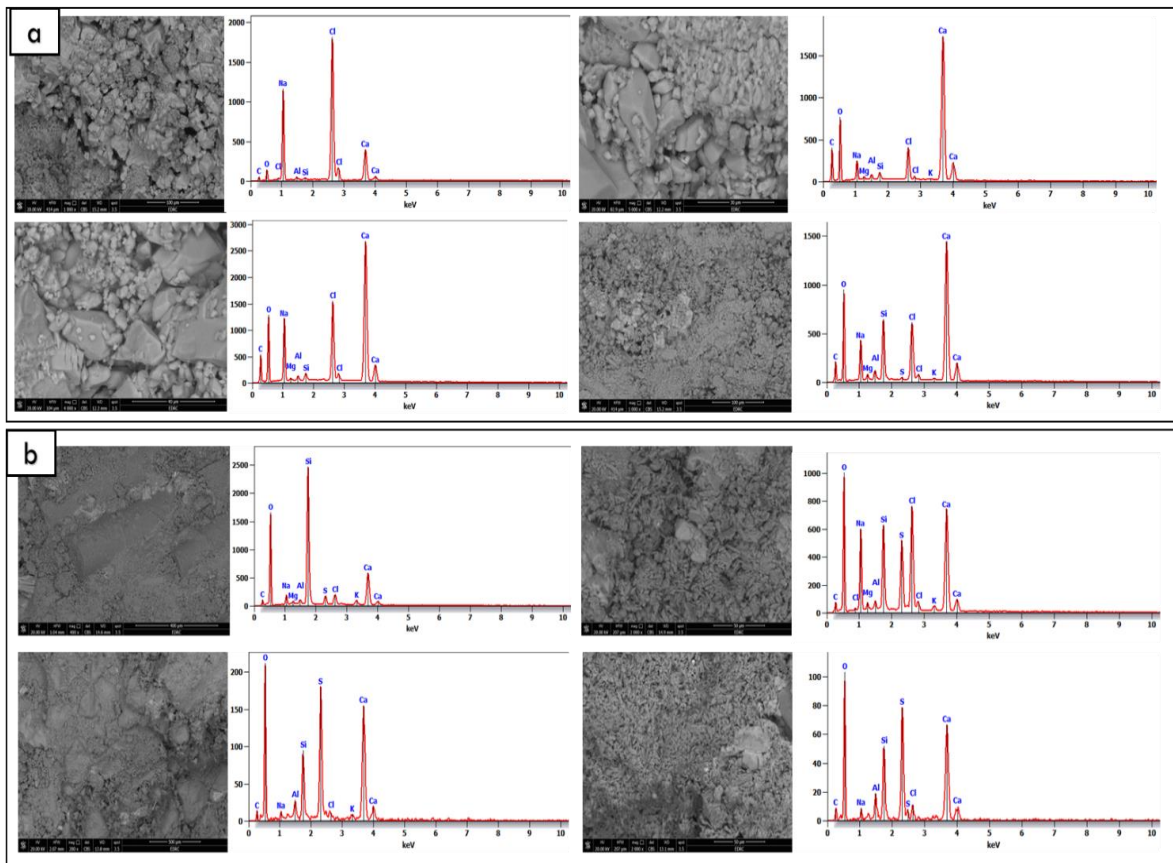


Fig .7. SEM photomicrographs and (EDX) microanalysis of (a) stone and (b) mortar samples (by the authors)

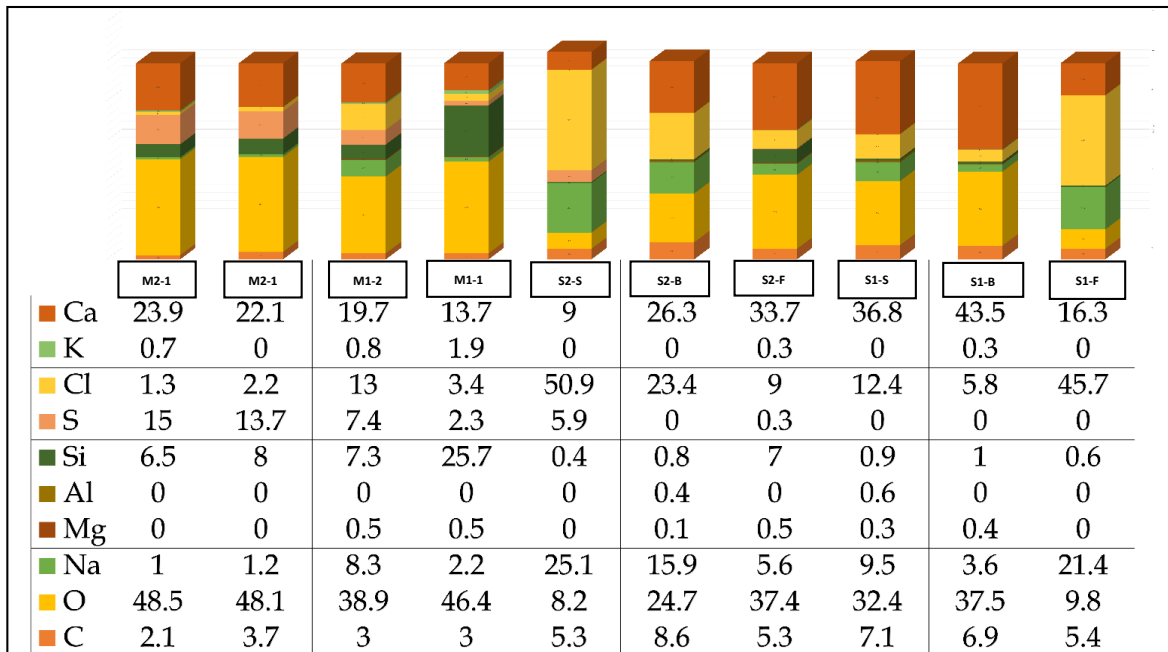
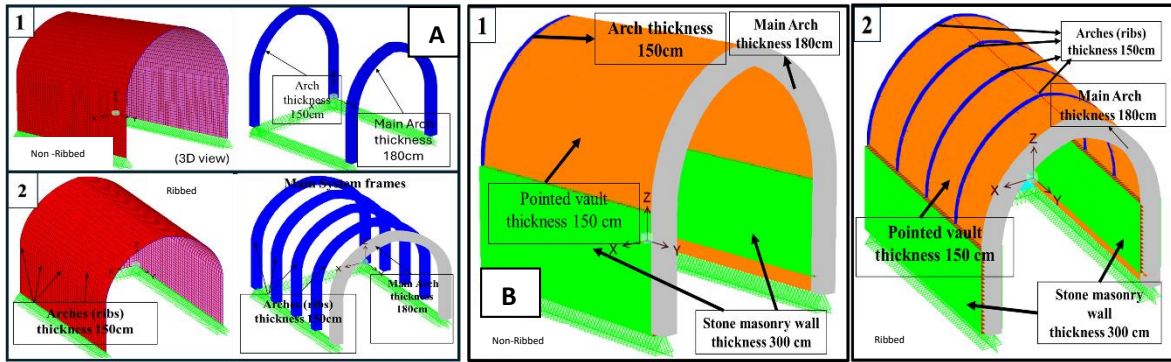


Fig.8. Weight percent (Wt. %) multi shots were taken per sample found for each element through the EDX area in the analyzed sample S)limestone (F-face)(B-Back)(S-Side); M) mortar. (by the authors)



A- 3D-View F.E. Main model 'shell' and 'frame' elements B-3D-View F.E. Main model solid-elements

Fig. 9. The main 3D numerical models of iwan: non-ribbed and ribbed. A) the model using 'shell' and 'frame' elements, while B) the models using solid elements (by the authors).

NO.	A) Shell – element models'		B) Solid – element models	
	No ribs	Ribbed	No ribs	Ribbed
1-Deflected shape				
2-Principal Stresses X direction (S11)				
3-Principal Stresses Y direction (S22)				
4-Principal Tensile Stress (Smax)				

Fig.10. Comparison of the structural analysis results under linear static load case of 3D numerical models for two types of iwan: non-ribbed and ribbed. A) depicts the results using 'shell' and 'frame' elements, while B) represents the results using solid elements (by the authors).

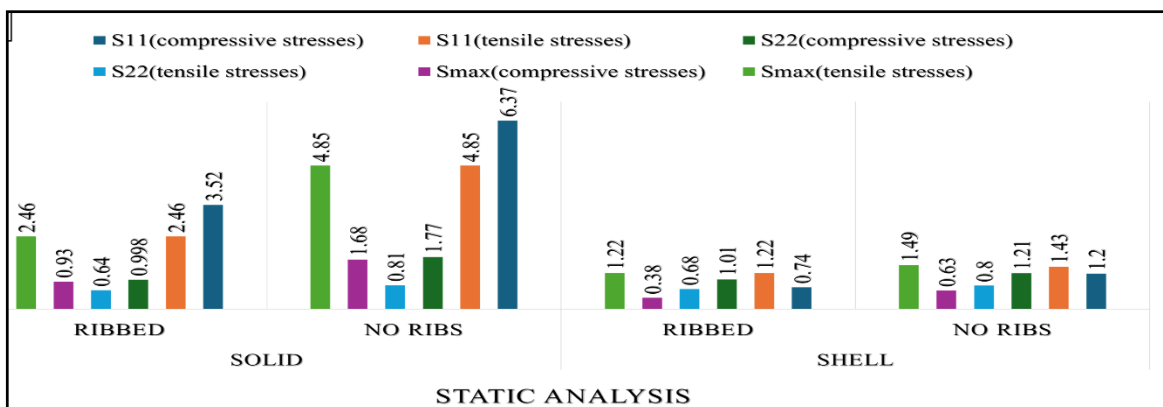


Fig. 11. Comparison of FE 3D model results under linear static analysis (i.e. dead load of self-weight (D.L.)) (by the authors).

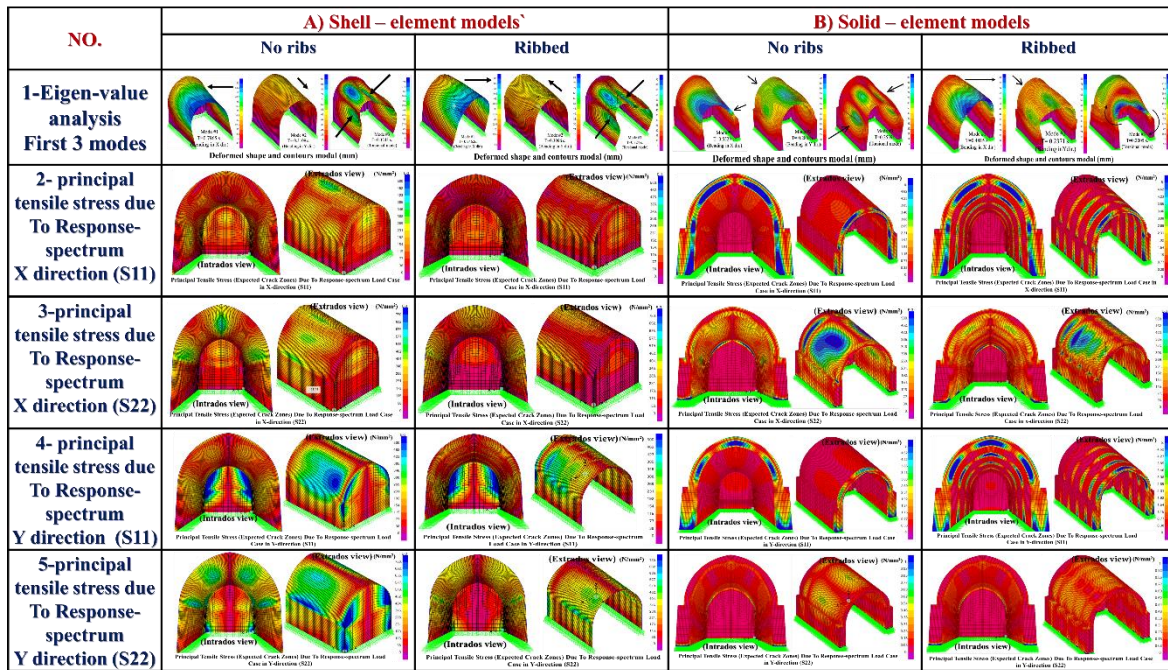


Fig.12. Comparison of the structural analysis results under dynamic analysis, such as eigenvalue and response spectrum in the X- and Y-directions. 3D numerical models for two types of iwan: non-ribbed and ribbed. A) depicts the results using 'shell' and 'frame' elements, while B) represents the results using solid elements (by the authors).

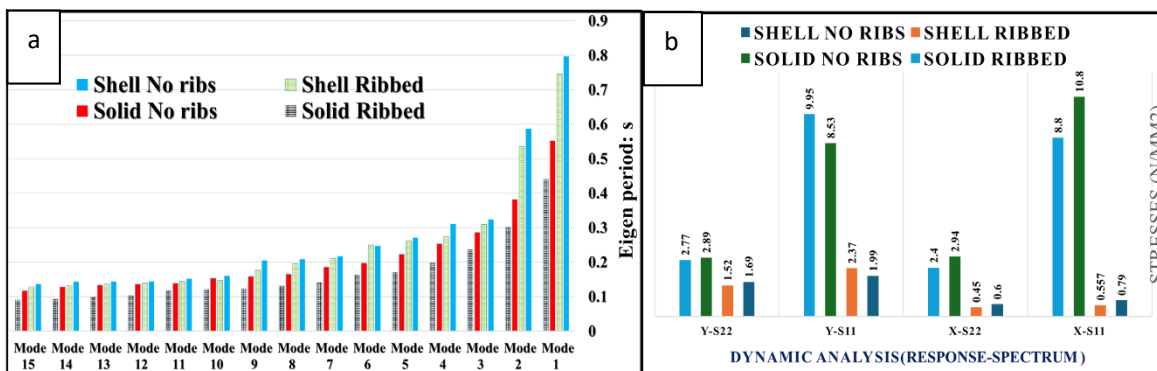


Fig.13. Comparison of major studied FE 3D models' results: a) eigenvalue periods for the first fifteen modes; b) response spectrum in the X- and Y-directions (by the authors).

التقييم الإنشائي للأقبية الأسطوانية المدعمة بالأضلاع في المباني الدينية خلال العصر المملوكي البحري: دراسة حالة على الإيوان الرئيسي لمدرسة السلطان حسن، القاهرة، مصر.

المخلص

تقدم هذه الورقة البحثية تقييماً هيكلياً للأقبية ذات الأضلاع المبنية من الطوب غير المسلح (UMRBV) في المباني الدينية للعصر المملوكي البحري في القاهرة التاريخية. يهدف البحث إلى تقييم الوظائف الإنشائية للأضلاع في هذه الأقبية من خلال مقارنة استقرارها الهيكلي تحت ظروف التحميل المتوقعة المختلفة مع الأقبية غير المضلعة. سيتم تطبيق التحليل الهيكلي المذكور على القبر الرئيسي في الإيوان الكبير لمدرسة السلطان حسن، حيث يُعتبر هذا الإيوان أكبر إيوانات القاهرة التاريخية.

ويبدأ البحث بدراسة تاريخية ومعمارية موجزة، ثم يجري تحقيقاً لمواد البناء المستخدمة في الإيوان باستخدام تقنيات **PLM** و **XRD** و **SEM-EDX**. وكما يتم إجراء تحليل إنشائي شامل باستخدام طريقة العناصر المحدودة (**F.E.M.**) على الإيوان عبر برامج هندسية معروفة. ويشمل البحث أيضاً تحليلاً مقارنةً لنماذج الإيوان، سواءً مع الأضلاع أو بدونها، باستخدام العناصر الصدفية ثلاثية الأبعاد والعناصر الصلبة ضمن البرنامج المختار.

أظهرت النتائج تحسناً كبيراً في الأداء الإنشائي للنماذج المضلعة مقارنةً بنظيراتها غير المضلعة. يتجلى هذا التحسن في انخفاض بنسبة تصل إلى ٤٦,٥% في الإزاحات، وانخفاض بنسبة تصل إلى ٤٤,٢% في الإجهادات، وذلك تحت ظروف التحميل الساكنة والديناميكية. بناءً على النتائج المستخلصة، سيتم اقتراح توصيات موجزة لطرق تدعيم الأقبية.

دعاء حسين^١

ياسر عبدالعاطي^٢

كلية الآثار، جامعة القاهرة

[1 doaae997@cu.edu.eg](mailto:1.doaae997@cu.edu.eg)

[2 yaser_yehya@cu.edu.eg](mailto:2.yaser_yehya@cu.edu.eg)

بيانات المقال

تاريخ المقال

تم الاستلام في ١٩ سبتمبر ٢٠٢٣
تم استلام النسخة المنقحة في ١٥ ابريل ٢٠٢٤

تم قبول البحث في ٣٠ يونيو ٢٠٢٤
متاح على الإنترنت في ٨ فبراير ٢٠٢٥

الكلمات الدالة

القبر الأسطواني، الأضلاع، البناء الحجري، الإيوان، التقييم، التدعيم